Large linear magnetoresistance in the Dirac semimetal TlBiSSe

Mario Novak,[*] Satoshi Sasaki, Kouji Segawa, and Yoichi Ando[†]

Institute of Scientific and Industrial Research, Osaka University, Ibaraki, Osaka 567-0047, Japan
(Received 25 July 2014; revised manuscript received 29 December 2014; published 20 January 2015)

The mixed-chalcogenide compound TlBiSSe realizes a three-dimensional (3D) Dirac semimetal state. In clean, low-carrier-density single crystals of this material, we found Shubnikov–de Haas oscillations to signify its 3D Dirac nature. Moreover, we observed very large linear magnetoresistance (MR) approaching 10 000% in 14 T at 1.8 K, which diminishes rapidly above 30 K. Our analysis of the magnetotransport data points to the possibility that the linear MR is fundamentally governed by the Hall field; although such a situation has been predicted for highly inhomogeneous systems, inhomogeneity does not seem to play an important role in TlBiSSe. Hence, the mechanism of large linear MR is an intriguing open question in a clean 3D Dirac system.

The discoveries of graphene [1] and three-dimensional (3D) topological insulators [2–4] have greatly advanced the research on two-dimensional (2D) massless Dirac fermions. In comparison, 3D massless Dirac fermions, whose Hamiltonian involves all three Pauli matrices, have attracted much less attention. This is due partly to the shortage of concrete materials to give access to the massless Dirac physics in 3D, although *massive* 3D Dirac fermions in Bi are long known to present interesting physics [5–7]. However, this situation has changed recently, and materials to realize 3D massless Dirac fermions are currently attracting significant attention because of the interest in new types of topological materials called Weyl semimetals [8,9]. In recent literature, materials realizing spin-degenerate 3D massless Dirac cones are called "3D Dirac semimetals," while those realizing a pair of spin-nondegenerate 3D massless Dirac cones are called "Weyl semimetals"; the latter is derived from the former by breaking time-reversal symmetry or space-inversion symmetry (or both) to split the spin-degenerate Dirac cone into two spin-nondegenerate ones [9].

Recently, the 3D Dirac semimetal phase has been shown to exist in Na_3Bi [10–12] and Cd_3As_2 [13–15], where the Dirac nodes are protected by crystal symmetry [16,17]. Also, such a phase is known to exist at the topological phase transition point of $TlBi(S_{1-x}Se_x)_2$ [18–21], $Pb_{1-x}Sn_xSe$ [22], $Bi_{1-x}Sb_x$ [23], etc., where the bulk band gap necessarily closes. In those materials, the Weyl semimetal phase would be realized by magnetic doping, breaking the crystal-inversion symmetry, or applying an external magnetic field [20,21,24,25]. Besides being potential parent materials of Weyl semimetals, the Dirac semimetals offer a new playground to explore the physics of massless Dirac fermions in larger spatial degrees of freedom than the 2D case, which may change the characteristic transport properties in a nontrivial way.

In this Rapid Communication, we report our magnetotransport studies of TlBiSSe, where the 3D Dirac semimetal phase is realized as a result of the topological phase transition between the topological insulator (TI) $TlBiSe_2$ and an ordinary insulator $TlBiS_2$ [18,19]. In TlBiSSe, as the Fermi level is tuned close to the Dirac point, the magnetoresistance (MR) grows very

rapidly, and its magnetic-field dependence is found to become linear in high magnetic fields. Surprisingly, in samples with a Fermi energy E_F of about 20 meV, we observed very large linear MR approaching 10 000% at 14 T. Our analysis of the magnetotransport data strongly suggests that the linear MR is somehow governed by the Hall field, but its origin is not explicable with existing theories for linear MR, pointing to different physics in 3D Dirac fermions than in the 2D case.

The topological phase transition in $TlBi(S_{1-x}Se_x)_2$ was discovered [18,19] soon after $TlBiSe_2$ was found to be a TI [26–28]. According to the angle-resolved photoemission spectroscopy (ARPES) data, the bulk band gap in $TlBi(S_{1-x}Se_x)_2$ closes at $x = 0.50$ [29], across which the band inversion and a change in the Z_2 topology takes place. This means that the zero-gap semimetallic state is realized in TlBiSSe, in which S and Se occupy the chalcogen site in a mixed way. In fact, a recent ARPES study gave direct evidence that TlBiSSe is a 3D Dirac semimetal [14]; a fluctuation of 0.005 in the composition x would allow a small gap of ~ 3 meV at the Dirac point [29], but this is much smaller than the E_F of our sample.

Single crystals of $TlBi(S_{1-x}Se_x)_2$ grown from stoichiometric melts are always n type with a typical carrier density of 10^{20} cm^{-3} [26]. Motivated by a recent report [30], we have grown crystals of TlBiSSe with a Tl-rich starting composition [31], and succeeded in reducing the bulk carrier density down to the 10^{17} cm^{-3} level. The high crystallinity of our single crystals is confirmed by x-ray diffraction (XRD) analysis [Fig. 1(a)] and Laue analysis. Although the crystals are grown from off-stoichiometric melts, inductively coupled plasma atomic-emission spectroscopy (ICP-AES) analysis confirmed that the compositions of the grown crystals are close to stoichiometry, and electron-probe microanalysis (EPMA) data assured that there is no segregation of constituent elements, as discussed in the Supplemental Material [31]. Experimental details of our transport measurements are also described in Ref. [31].

The temperature dependencies of the in-plane resistivity $\rho_{xx}(T)$ of three representative TlBiSSe samples with significantly different carrier densities are shown in Fig. 1(b); note that the vertical axis is in a logarithmic scale, and the residual resistivity ratio of the lowest-carrier-density sample (S3) is as large as 73. We have actually measured many more samples than are shown in Fig. 1(b), and Fig. 1(c)
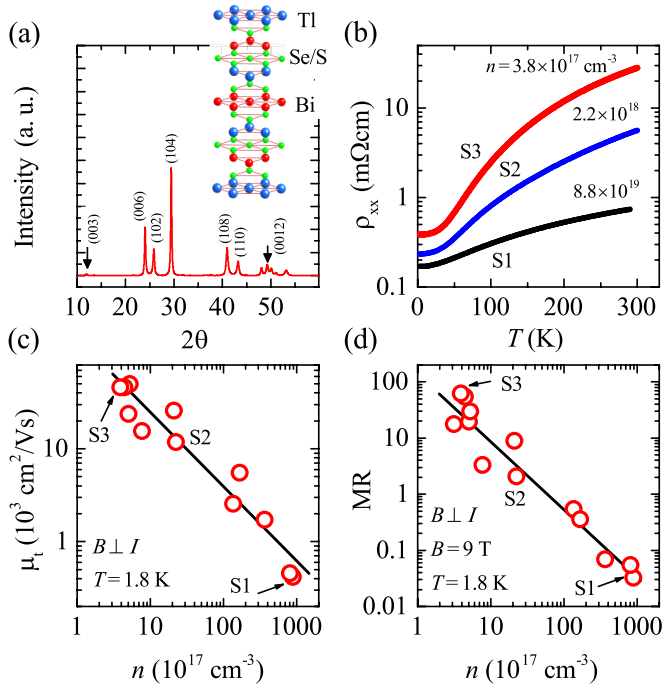

FIG. 1. (Color online) (a) Powder XRD pattern of a typical TlBiSSe crystal; the inset shows its crystal structure. (b) $\rho_{xx}(T)$ behavior of three samples with different carrier densities. (c), (d) Plots of low-temperature mobility and the magnitude of MR vs n. The MR values shown here are for 9 T at 1.8 K.
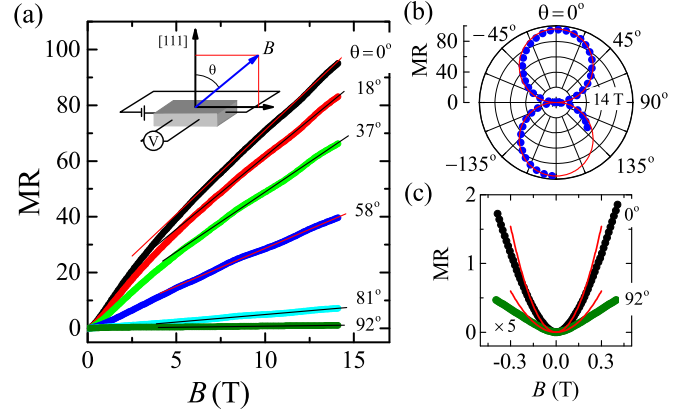

FIG. 2. (Color online) MR in sample S3 at 1.8 K. (a) $\rho_{xx}(B)$ behavior for various magnetic-field angles from transverse ($\theta = 0°$, B field in the [111] direction) to the near-longitudinal ($\theta = 92°$) configurations; the inset depicts the definition of θ. (b) Dipolelike θ dependence of the magnitude of MR at 14 T, which follows the $\cos\theta$ dependence (red solid line). Due to the restriction of the rotation stage, the range of θ does not span the whole 360°. (c) Low-field MR showing ordinary B^2 behavior; the red solid lines show the fits to the B^2 function.

shows that the low-temperature transport mobility μ_t (assessed from ρ_{xx} at 1.8 K and the carrier density n) increases systematically with decreasing n; for example, μ_t increases by 110 times between samples S1 ($n = 8.8 \times 10^{19}$ cm^{-3}) and S3 ($n = 3.8 \times 10^{17}$ cm^{-3}). This is in contrast to the case of 2D Dirac systems such as graphene [32] and 3D TIs [33], where μ_t shows an enhancement only when the Fermi level is tuned very close to the Dirac point.

Perhaps more surprising is the very rapid increase in MR with decreasing n; for example, the MR at 9 T [Fig. 1(d)] changes by almost 2000 times between S1 and S3. Here, MR is defined by $[\rho_{xx}(B) - \rho_{xx}(0\,\mathrm{T})]/\rho_{xx}(0\,\mathrm{T})$. To gain insights into the large MR, Fig. 2(a) shows how the MR behavior in sample S3 changes when the magnetic field is tilted from the perpendicular to parallel directions. The angular dependence is more directly shown in Fig. 2(b), where the magnitude of the MR in 14 T is plotted as a function of the angle θ, which is defined in the inset of Fig. 2(a). The dipolelike pattern seen in Fig. 2(b) is well described by the $\cos\theta$ function (red solid line), meaning that the MR is almost entirely governed by the perpendicular component of the magnetic field, even though the present system is 3D. The magnetic-field dependence of ρ_{xx} at low field is plotted in Fig. 2(c) for $\theta = 0°$ and 92°, both of which present the ordinary B^2 behavior below ∼0.1 T; this suggests that the origin of the linear MR is different from the famous linear MR in Ag$_{2+\delta}$Se and Ag$_{2+\delta}$Te [34], where the linearity is observed from as low as 1 mT. Note that, due to the high mobility of sample S3, the condition $\omega_c\tau_t = \mu_t B = 1$ (τ_t is the transport scattering time and $\omega_c = eB/m_c$ is the cyclotron frequency with m_c the cyclotron mass) is achieved

in only 0.2 T, and hence the standard theory for MR for a closed Fermi surface [35] would predict a saturation at $B \gg 0.2$ T; nevertheless, as one can see in Fig. 2(a), this sample presents nonsaturating linear MR above ∼6 T.

The temperature dependence of this linear MR signifies its unique nature in comparison to other systems showing large linear MR [34,36–40]. Figures 3(a)–3(c) show ρ_{xx} vs B at various temperatures, where one can see that the characteristic field above which the linear MR is observed remains around 6 T up to 150 K, but at higher temperatures the linear MR disappears. More importantly, the size of MR changes little between 1.8 and 30 K, but at higher temperatures it diminishes rapidly. This temperature dependence is summarized in Fig. 3(d), where the dependence of n on temperature is plotted together; one can see that n changes only by a small amount, and hence the rapid decline in MR has little to do with the thermal activation of carriers. On the other hand, as shown in Fig. 3(e), the size of MR depends linearly on μ_t, implying that the reason for the rapid decline in MR is the phonon scattering which restricts μ_t at high temperatures.

It is prudent to mention that, even though the MR is unusual in many respects, it obeys the Kohler's rule [35] (see Ref. [31] for details), meaning that ρ_{xx} depends on the magnetic field only through the form $B\tau_t$ (which is the case in the semiclassical relaxation-time approximation). In passing, the MR data at 200 and 300 K can be described by the conventional form $aB^2/(1 + bB^2)$ [41].

The low-carrier-density samples are clean enough to present Shubnikov–de Haas (SdH) oscillations, which are the source of the wiggles in the MR data at high B. The clear observation of SdH oscillations signifies not only a high mobility but also a high homogeneity of local carrier densities, since a variation in the local carrier density would result in a spread of SdH frequencies to smear the oscillations. In the case of TlBiSSe, a larger number of oscillation cycles are discernible
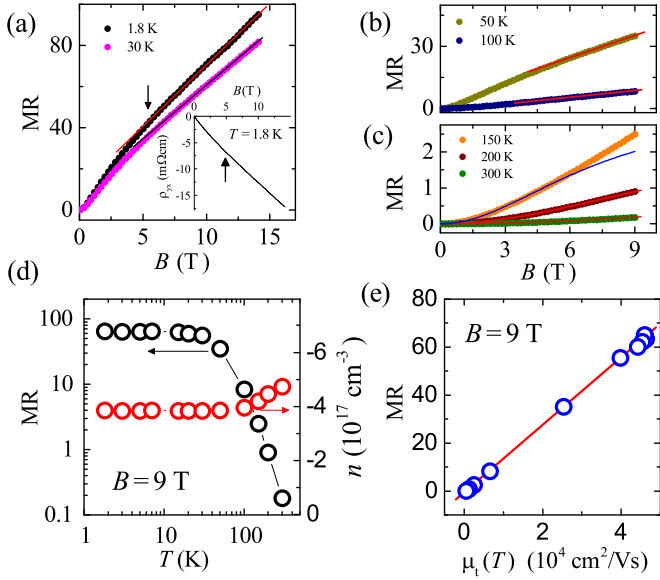
FIG. 3. (Color online) MR in sample S3 for $\theta = 0°$. (a)–(c) $\rho_{xx}(B)$ behavior at various temperatures; note the different vertical scales between the panels. The inset in (a) shows the $\rho_{yx}(B)$ behavior at 1.8 K; the arrows mark the change in slope. The straight lines in (a) and (b) are fits to the linear part, while the solid lines in (c) are fits of the low-field part to the classical $aB^2/(1 + bB^2)$ law. (d) Temperature dependences of the magnitude of MR at 9 T (left axis) and the carrier density calculated from R_H at each T (right axis). (e) Plot of the magnitude of MR at 9 T vs the transport mobility μ_t, which changes with T.
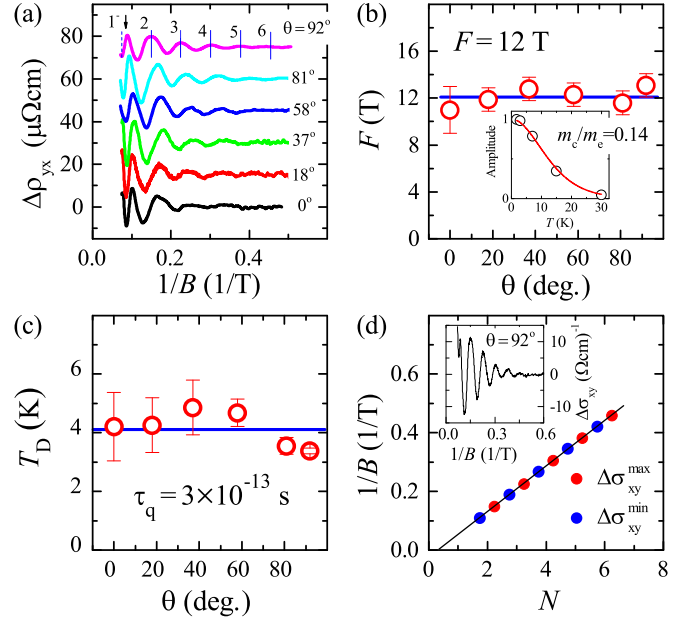

FIG. 4. (Color online) SdH oscillations in sample S3. (a) SdH oscillations in ρ_{yx} vs $1/B$ at 1.8 K for various magnetic-field directions. The equidistant maxima are indicated by vertical lines, with the exception of the first Landau level which shows spin splitting, giving a g factor of 6 [31]. (b) θ dependence of the oscillation frequency; the inset shows the temperature dependence of the oscillation amplitude for $\theta = 0°$, together with the fitting to the Lifshitz-Kosevich theory which gives $m_c/m_e = 0.14$. (c) θ dependence of the Dingle temperature. (d) Landau-level index plot for oscillations in σ_{xy} measured at 1.8 K and $\theta = 0°$; the inset shows the oscillations in $\Delta\sigma_{xy}$ which are obtained by subtracting a smooth background from σ_{xy}. Following the principle in Refs. [4,47] and assuming electron carriers, we assign the indexes $N + \frac{1}{4}$ and $N + \frac{3}{4}$ to the maxima and minima in $\Delta\sigma_{xy}$, respectively. The solid line is a linear fitting to the data, giving the intercept on the N axis of 0.34.

in $\rho_{yx}(B)$ than in $\rho_{xx}(B)$, so we mainly used the former for the following analysis. Figure 4(a) shows SdH oscillations in ρ_{yx} for varying magnetic-field angles θ after removing the linear background. The Fourier transform gives only one frequency, whose dependence on θ is shown in Fig. 4(b); these data reveal a very small spherical (isotropic) Fermi surface (FS).

The averaged frequency $F = 12$ T gives the FS radius $k_F^{3D} = 1.9 \times 10^6$ cm^{-1} and the carrier density $n_{SdH} = 2.4 \times 10^{17}$ cm^{-3} [42]. From the temperature dependence of the oscillation amplitude at $\theta = 0°$ [Fig. 4(b) inset], we obtain $m_c = 0.14m_e$ (m_e is the free electron mass) by using the Lifshitz-Kosevich (LK) theory [43]. This allows us to determine the Dingle temperature T_D, which is plotted in Fig. 4(c) as a function of θ. Its average value, $T_D = 4.1$ K, gives the quantum scattering time $\tau_q = \hbar/(2\pi k_B T_D) = 3 \times 10^{-13}$ s. This is to be compared with the transport scattering time $\tau_t = 3.7 \times 10^{-12}$ s assessed from μ_t; the difference, which in this case is about ten times, is usually associated with the difference in the rates between forward and backward scatterings [44]; apparently, small-angle (forward) scatterings are predominant in TlBiSSe, which happens when scattering is mainly due to weak disorder. Other parameters of interest are obtained as follows: the quantum mobility $\mu_q \equiv e\tau_q/m_c \approx 3500$ cm^2/V s, Fermi velocity $v_F = \hbar k_F/m_c = 1.6 \times 10^5$ m/s, and the Fermi energy (measured from the Dirac point) $E_F = \hbar v_F k_F = 20$ meV.

Important information derived from SdH oscillations is the Berry phase [4,45,46]. We made the Landau-level (LL) index plot based on the positions of minima and maxima in σ_{xy} [47] as a function of $1/B$ [Fig. 4(d) inset]. In a system with 3D

FS, the intercept of the index plot on the N axis is expected to be $0 \pm 1/8$ for Schrödinger fermions, while it should be $1/2 \pm 1/8$ for Dirac fermions (the sign before $1/8$ should be $+$ for holes and $-$ for electrons) [45,46]. In our case, the intercept is 0.34 [Fig. 4(d)], which is close to $1/2 - 1/8 = 0.375$ and hence is consistent with 3D Dirac electrons.

We now discuss the possible mechanism of the observed large linear MR. There are several theoretical models which predict linear MR for low-carrier-density systems. Abrikosov [48,49] proposed a quantum interpretation of the phenomena by assuming the system to be in the ultraquantum limit. In our sample S3, the linear MR in the transverse orientation ($\theta = 0°$) sets in at ~6 T, which corresponds to the situation when the Fermi level is in the second LL; such a situation was previously argued to be sufficiently close to the ultraquantum limit to observe the quantum linear MR [36–38], and hence at first sight the Abrikosov's model seems applicable. However, an important prediction of the model is that the linear MR should be stable against temperature as long as the thermal broadening of the LLs is smaller than their separation, which is given by the cyclotron energy $\hbar\omega_c$; in the present case, $\hbar\omega_c$ in 14 T is 133 K, whereas a strong decrease in the

MR occurs above $\sim$30 K [Fig. 3(d)], which speaks against the validity of the Abrikosov's model.

Thus we turn to other models which can predict linear nonsaturating MR in a system with small 3D FS. A classical one is by Herring [50], who developed a perturbation theory for a system with weak inhomogeneity in the carrier density and showed that the fluctuations in the Hall field will lead to linear MR. Parish and Littlewood (PL) [51,52] proposed a model which is valid also in the strong inhomogeneity limit and showed that the inhomogeneity will cause distortions in the current paths, which in turn causes the Hall field to contribute to the MR. In this regard, the θ dependence of the MR [Fig. 2(b)], which suggests that only the perpendicular component of the magnetic field is responsible for the MR, seems to support the scenario that the linear MR originates from the Hall field. Moreover, the data for in-plane magnetic field rotation (described in the Supplemental Material [31]) are also consistent with this scenario. In addition, it is suggestive that a change in slope of $\rho_{xx}(B)$ that occurs at around 5 T seems to be correlated with a similar change in slope of $\rho_{yx}(B)$ at the same field [Fig. 3(a)].

An important clue comes from the Hall angle $\theta_{\rm H}$. According to the semiclassical theory for a single-band metal, the relation $\tan\theta_H = \rho_{yx}/\rho_{xx} = \sigma_{xy}/\sigma_{xx} = \omega_c\tau_t$ should hold. However, if we calculate these values for sample S3 in 14 T, $\tan\theta_H = \rho_{yx}/\rho_{xx} = 0.5$, whereas $\omega_c\tau_t = \mu_t B = 65$. Therefore, there is a two orders-of-magnitude difference between what is purported to be the same parameter. This is significant, and it strongly supports the scenario that MR is actually governed by the Hall field rather than the scattering.

In the PL and Herring's model, the existence of inhomogeneity is essential. However, in our samples, good crystallinity and the absence of compositional segregations were confirmed by x-ray and EPMA analyses, respectively [31]. Also, the average donor distance $l_{\rm imp} \simeq n_{\rm SdH}^{-1/3} = 15$ nm and the Debye screening length $l_{\rm Debye} = 3$ nm [53] are both short; thus, the low temperature mean free path $\ell = v_F\tau_t = 600$ nm does not support the impurities to be the source of strong inhomogeneity. While the linear relation between MR and μ_t [Fig. 3(e)] is along the lines with the prediction of the PL model, the decline of the mobility in this case is due to phonon scattering and is not related to inhomogeneity. Therefore, while the Hall field appears to be the fundamental source of the linear

MR, the actual mechanism to bring about such a situation is an open question. It is fair to note that the magnetoresistance behavior in narrow- or zero-gap semiconductors are generally not well understood, but the phenomenology in the present case is a unique one.

Finally, we mention that in a recent work on another 3D Dirac system, Cd_3As_2, gigantic MR was found in high-mobility samples (with $\mu_t > 10^7$ cm^2/V s) [54]. This effect stems from a mysterious protection from backscattering [55] that is strong only along k_x, as reflected in the large resistivity anisotropy $\rho_{yy}/\rho_{xx} \simeq 30$. In multidomain samples with $\mu_t \simeq 10^4$ cm^2/V s, large linear MR was observed, but it starts from a very low field and it persists to 300 K, both of which suggest that it is in line with the PL model. Importantly, even in the high-mobility Cd_3As_2 samples, τ_q (which reflects lattice disorder) is ten times *shorter* than in TlBiSSe, suggesting that Cd_3As_2 is inherently dirtier due to lattice disorder [54]. Hence, the transport in Cd_3As_2 is apparently complicated by material-specific issues. In contrast, TlBiSSe does not present mysterious protection from backscattering, its lattice is much cleaner, and it has only one Dirac node, all of which suggest that TlBiSSe is a simpler system to study the generic properties of 3D Dirac fermions.

In summary, we found that in the 3D Dirac semimetal TlBiSSe, a reduction in carrier density n leads to a rapid increase in the transport mobility μ_t and transverse magnetoresistance (MR). In samples with $n \simeq 10^{17}$ cm^{-3}, μ_t becomes 5×10^4 cm^2/V s and linear MR whose magnitude reaches almost 10 000% in 14 T was observed at 1.8 K. This linear MR is governed by the perpendicular component of the magnetic field, and the large discrepancy between $\tan\theta_H$ and $\omega_c\tau_t$ points to the scenario that the Hall field is the fundamental source of the linear MR. Nevertheless, inhomogeneity does not seem to play an important role here, and the exact mechanism to produce the large liner MR is yet to be elucidated.

---

[1] A. K. Geim and K. S. Novoselov, Nat. Mater. **6**, 183 (2007).

[2] M. Z. Hasan and C. L. Kane, Rev. Mod. Phys. **82**, 3045 (2010).

[3] X.-L. Qi and S.-C. Zhang, Rev. Mod. Phys. **83**, 1057 (2011).

[4] Y. Ando, J. Phys. Soc. Jpn. **82**, 102001 (2013).

[5] H. Fukuyama, Y. Fuseya, M. Ogata, A. Kobayashi, and Y. Suzumura, Physica B **407**, 1943 (2012).

[6] L. Li, J. G. Checkelsky, Y. S. Hor, C. Uher, A. F. Hebard, R. J. Cava, and N. P. Ong, Science **321**, 547 (2008).

[7] Z. Zhu, A. Collaudin, B. Fauque, W. Kang, and K. Behnia, Nat. Phys. **8**, 89 (2012).

[8] X. Wan, A. M. Turner, A. Vishwanath, and S. Y. Savrasov, Phys. Rev. B **83**, 205101 (2011).

[9] O. Vafek and A. Vishwanath, Annu. Rev. Condens. Matter Phys. **5**, 83 (2014).

[10] Z. Wang, Y. Sun, X.-Q. Chen, C. Franchini, G. Xu, H. Weng, X. Dai, and Z. Fang, Phys. Rev. B **85**, 195320 (2012).

[11] Z. K. Liu, B. Zhou, Y. Zhang, Z. J. Wang, H. M. Weng, D. Prabhakaran, S.-K. Mo, Z. X. Shen, Z. Fang, X. Dai, Z. Hussain, and Y. L. Chen, Science **343**, 864 (2014).

[12] S.-Y. Xu, C. Liu, S. K. Kushwaha, T.-R. Chang, J. W. Krizan, R. Sankar, C. M. Polley, J. Adell, T. Balasubramanian, K. Miyamoto, N. Alidoust, G. Bian, M. Neupane, I. Belopolski, H.-T. Jeng, C.-Y. Huang, W.-F. Tsai, H. Lin, F. C. Chou, T. Okuda, A. Bansil, R. J. Cava, and M. Z. Hasan, arXiv:1312.7624.

[13] Z. Wang, H. Weng, Q. Wu, X. Dai, and Z. Fang, Phys. Rev. B **88**, 125427 (2013).

[14] M. Neupane, S.-Y. Xu, R. Sankar, N. Alidoust, G. Bian, C. Liu, I. Belopolski, T.-R. Chang, H.-T. Jeng, H. Lin, A. Bansil, F. Chou, and M. Z. Hasan, Nat. Commun. **5**, 3786 (2014).

[15] S. Borisenko, Q. Gibson, D. Evtushinsky, V. Zabolotnyy, B. Büchner, and R. J. Cava, Phys. Rev. Lett. **113**, 027603 (2014).

[16] S. M. Young, S. Zaheer, J. C. Y. Teo, C. L. Kane, E. J. Mele, and A. M. Rappe, Phys. Rev. Lett. **108**, 140405 (2012).

[17] B.-J. Yang and N. Nagaosa, Nat. Commun. **5**, 4898 (2014).

[18] T. Sato, K. Segawa, K. Kosaka, S. Souma, K. Nakayama, K. Eto, T. Minami, Y. Ando, and T. Takahashi, Nat. Phys. **7**, 840 (2011).

[19] S.-Y. Xu, Y. Xia, L. A. Wray, S. Jia, F. Meier, J. H. Dil, J. Osterwalder, B. Slomski, A. Bansil, H. Lin, R. J. Cava, and M. Z. Hasan, Science **332**, 560 (2011).

[20] A. A. Burkov and L. Balents, Phys. Rev. Lett. **107**, 127205 (2011).

[21] B. Singh, A. Sharma, H. Lin, M. Z. Hasan, R. Prasad, and A. Bansil, Phys. Rev. B **86**, 115208 (2012).

[22] I. Zeljkovic, Y. Okada, M. Serbyn, R. Sankar, D. Walkup, W. Zhou, M. Z. Hasan, F. Chou, L. Fu, and V. Madhavan, arXiv:1403.4906.

[23] J. C. Y. Teo, L. Fu, and C. L. Kane, Phys. Rev. B **78**, 045426 (2008).

[24] H.-J. Kim, K.-S. Kim, J.-F. Wang, M. Sasaki, N. Satoh, A. Ohnishi, M. Kitaura, M. Yang, and L. Li, Phys. Rev. Lett. **111**, 246603 (2013).

[25] D. Bulmash, C.-X. Liu, and X.-L. Qi, Phys. Rev. B **89**, 081106(R) (2014).

[26] T. Sato, K. Segawa, H. Guo, K. Sugawara, S. Souma, T. Takahashi, and Y. Ando, Phys. Rev. Lett. **105**, 136802 (2010).

[27] K. Kuroda, M. Ye, A. Kimura, S. V. Eremeev, E. E. Krasovskii, E. V. Chulkov, Y. Ueda, K. Miyamoto, T. Okuda, K. Shimada, H. Namatame, and M. Taniguchi, Phys. Rev. Lett. **105**, 146801 (2010).

[28] Y. L. Chen, Z. K. Liu, J. G. Analytis, J.-H. Chu, H. J. Zhang, B. H. Yan, S.-K. Mo, R. G. Moore, D. H. Lu, I. R. Fisher, S. C. Zhang, Z. Hussain, and Z.-X. Shen, Phys. Rev. Lett. **105**, 266401 (2010).

[29] S.-Y. Xu, M. Neupane, C. Liu, S. Jia, L. A. Wray, G. Landolt, B. Slomski, J. H. Dil, N. Alidoust, S. Basak, H. Lin, J. Osterwalder, A. Bansil, R. J. Cava, and M. Z. Hasan, arXiv:1204.6518.

[30] K. Kuroda, G. Eguchi, K. Shirai, M. Shiraishi, M. Ye, K. Miyamoto, T. Okuda, S. Ueda, M. Arita, H. Namatame, M. Taniguchi, Y. Ueda, and A. Kimura, arXiv:1308.5521.

[31] See Supplemental Material at http://link.aps.org/supplemental/10.1103/PhysRevB.91.041203 for supplemental data and discussions.

[32] Y. Zhang, Y.-W. Tan, H. L. Stormer, and P. Kim, Nature (London) **438**, 201 (2005).

[33] F. Yang, A. A. Taskin, S. Sasaki, K. Segawa, Y. Ohno, K. Matsumoto, and Y. Ando, Appl. Phys. Lett. **104**, 161614 (2014).

[34] R. Xu, A. Husmann, T. F. Rosenbaum, M.-L. Saboungi, J. E. Enderby, and P. B. Littlewood, Nature (London) **390**, 57 (1997).

[35] A. A. Abrikosov, *Fundamentals of the Theory of Metals* (North-Holland, Amsterdam, 1988).

[36] J. Hu and T. F. Rosenbaum, Nat. Mater. **7**, 697 (2008).

[37] X. Wang, Y. Du, S. Dou, and C. Zhang, Phys. Rev. Lett. **108**, 266806 (2012).

[38] A. L. Friedman, J. L. Tedesco, P. M. Campbell, J. C. Culbertson, E. Aifer, F. K. Perkins, R. L. Myers-Ward, J. K. Hite, C. R. Eddy, Jr., G. G. Jernigan, and D. K. Gaskill, Nano Lett. **10**, 3962 (2010).

[39] N. A. Porter and C. H. Marrows, Sci. Rep. **2**, 565 (2012).

[40] N. V. Kozlova, N. Mori, O. Makarovsky, L. Eaves, Q. D. Zhuang, A. Krier, and A. Patane, Nat. Commun. **3**, 1097 (2012).

[41] A. B. Pippard, *Magnetoresistance in Metals* (Cambridge University Press, Cambridge, UK, 1989).

[42] The carrier density determined from the low-field R_H for the sample S3 is $n = 3.8 \times 10^{17}$ cm^{-3}.

[43] D. Shoenberg, *Magnetic Oscillations in Metals* (Cambridge University Press, Cambridge, UK, 1984).

[44] S. Das Sarma and F. Stern, Phys. Rev. B **32**, 8442 (1985).

[45] I. A. Luk'yanchuk and Y. Kopelevich, Phys. Rev. Lett. **97**, 256801 (2006).

[46] H. Murakawa, M. S. Bahramy, M. Tokunaga, Y. Kohama, C. Bell, Y. Kaneko, N. Nagaosa, H. Y. Hwang, and Y. Tokura, Science **342**, 1490 (2013).

[47] A. A. Taskin, F. Yang, S. Sasaki, K. Segawa, and Y. Ando, Phys. Rev. B **89**, 121302(R) (2014).

[48] A. A. Abrikosov, Phys. Rev. B **58**, 2788 (1998).

[49] A. A. Abrikosov, Europhys. Lett. **49**, 789 (2000).

[50] C. Herring, J. Appl. Phys. **31**, 1939 (1960).

[51] M. M. Parish and P. B. Littlewood, Nature (London) **426**, 162 (2003).

[52] J. Hu, M. M. Parish, and T. F. Rosenbaum, Phys. Rev. B **75**, 214203 (2007).

[53] The Debye screening length $l_{\mathrm{Debye}} = [\epsilon k_B T/(ne^2)]^{1/2} = 3$ nm is for the dielectric constant $\epsilon \approx 20$ and $T = 1.8$ K.

[54] T. Liang, Q. Gibson, M. N. Ali, M. Liu, R. J. Cava, and N. P. Ong, Nat. Mater. (2014).

[55] Electrons in 3D Dirac semimetals do not have helical spin polarization to protect them from backscattering.